Effect of the ostreolysin A/pleurotolysin B pore-forming complex on neuroblastoma cell morphology and intracellular Ca^{2+} activity.

Milka Vrecl, Monika Babnik, Uroš Diacci, Evelyne Benoit, Robert Frangež

Effect of the ostreolysin A/pleurotolysin B pore-forming complex on neuroblastoma cell morphology and intracellular Ca^{2+} activity

Milka Vrecl [1], Monika Babnik [2], Uroš Diacci[2], Evelyne Benoit[3] and Robert Frangež[2]

[1]*Veterinary Faculty, Institute of Anatomy, Histology and Embryology, University of Ljubljana, Gerbičeva 60, SI-1000, Ljubljana, Slovenia*

[2]*Institute of Physiology, Pharmacology and Toxicology, Veterinary Faculty, University of Ljubljana, Gerbičeva 60, 1000 Ljubljana, Slovenia*

[3]*CNRS, Institut de Neurobiologie Alfred Fessard, Laboratoire de Neurobiologie et Développement bât. 32-33, 91198 Gif sur Yvette cedex, France*

*Corresponding author:

Robert Frangež; *E-mail address: robert.frangez@vf.uni-lj.si; Tel.: +386 1 477 91 31*

ABSTRACT

Ostreolysin A (OlyA) and pleurotolysin B (PlyB), isolated from edible oyster mushrooms, form a cytolytic complex (OlyA/PlyB) in membrane cells that causes respiratory arrest. This study evaluated the mechanisms underlying cytotoxic OlyA/PlyB activity in neuroblastoma NG108-15 cells. Confocal microscopy with morphometric analysis revealed that OlyA/PlyB increased the three-dimensional projected area of differentiated cells. Iso-osmotic replacement of NaCl by sucrose or Na-isethionate prevented the cellular swelling. This suggests that formation of cellular edema requires the presence of Na^+ and/or Cl^- in the extracellular space and may be related to an influx of Na^+ and/or a shift in Cl^-, which induce a marked influx of water that is ultimately responsible for cellular swelling. In addition, extracellular Ca^{2+} moderately contributed to the swelling because benzamil (10 μM), a $3Na^+/Ca^{2+}$ exchange (NCX) inhibitor, and Ca^{2+}-free medium partially prevented this response. Fluorometric measurements revealed that OlyA/PlyB, at approximately 15-fold higher concentrations, increased the intracellular Ca^{2+} activity $[Ca^{2+}]_i$. This increase was dependent on the presence of Na^+ and Ca^{2+} in the external medium and was sensitive to benzamil. It is thus likely that a switch in the NCX mode, associated with the *de novo* formation of non-selective ion pores by OlyA/PlyB in cellular plasma membranes, plays an important role in this effect. Overall, OlyA/PlyB affects neuroblastoma cell morphology and Ca^{2+} homeostasis to influence the toxin-induced respiratory arrest.

Key words: $[Ca^{2+}]_i$; MACPF domain; neuroblastoma NG108-15 cells; ostreolysin A; pleurotolysin B; cellular swelling

INTRODUCTION

Ostreolysin A (Oly A) and pleurotolysin B (PlyB), purified from the oyster mushroom (*Pleurotus ostreatus*), form a binary pore-forming cytolytic protein complex (OlyA/PlyB) (Berne *et al.*, 2002; Ota *et al.*, 2014; Ota *et al.*, 2013). The biological and toxic activity of this complex is a consequence of an interaction between the two proteins, the 15-kDa Oly A and the ~59-kDa Ply B, which contains a (membrane attack complement/perforin) MACPF domain (Gilbert *et al.*, 2013; Ota *et al.*, 2013). The binding of OlyA, which belongs to the aegerolysin protein family (NCBI: Pfam 06355) (Berne *et al.*, 2009), to membranes is a prerequisite for PlyB recruitment and the formation of the transmembrane pores (Ota *et al.*, 2014; Ota *et al.*, 2013; Schlumberger *et al.*, 2014). OlyA (and consequently also OlyA/PlyB) specifically recognizes and binds to raft-like, cholesterol- and sphingomyelin-enriched membrane microdomains (Rebolj *et al.*, 2010; Rebolj *et al.*, 2006; Sepcic *et al.*, 2004). Although the edible oyster mushroom is a widely cultivated species, sporadic acute intoxications have been described in humans and animals after the ingestion of large quantities of fresh mushrooms. A *P. ostreatus* water extract induces hemorrhage in the gastrointestinal tract, lungs and kidneys, and degenerative changes in the livers of mice challenged with these proteins have suggested that the described pathological alterations were produced by a thermolabile proteinaceous molecule(s), with an LD_{50} higher than 3000 μg/kg (Al-Deen *et al.*, 1987).

Toxicological studies have revealed that the OlyA/PlyB complex causes cardiac arrhythmias and cardiorespiratory arrest in rodents. In male mice, an acute LD_{50} of 1170 μg/kg was reported (Zuzek *et al.*, 2006). OlyA/PlyB was also shown to induce a concentration-dependent increase in aortic ring tension (Juntes *et al.*, 2009; Rebolj *et al.*, 2007). The OlyA/PlyB complex is composed of two large proteins and was previously thought to be unable to cross the blood-brain barrier. However, OlyA/PlyB produces a pore with a functional radius of > 2 nm, allowing calcium and other ions to pass through cellular membranes (Schlumberger *et al.*, 2014; Sepcic *et al.*, 2003). Osmotic shock may be responsible for the disruption of the cellular membranes and for the cytolytic effects of the protein complex (Berne *et al.*, 2005; Schlumberger *et al.*, 2014)). Due to its cytolytic nature, this complex may also damage the blood-brain barrier and enter the brain, inducing respiratory arrest. Indirect evidence supporting such a scenario includes the observation of OlyA/PlyB-induced histopathological lesions, including endothelium detachment in aorta and perivascular edema, in parenterally exposed rats (Juntes *et al.*, 2009). Additionally, some pore-forming bacterial toxins could also compromise the integrity of the endothelial layer *in vivo,* as shown for *S. pneumonie* pneumolysin (Hirst *et al.*, 2004; Orihuela *et al.*, 2004) and *C. perfringens* Ɛ-toxin (Nagahama and Sakurai, 1991; Soler-Jover *et al.*, 2004).

This work aimed to examine whether OlyA/PlyB affects the neuronal physiology that underlies respiratory arrest *in vivo* by determining whether the complex alters the morphology and calcium homeostasis of the neuroblastoma NG108-15 cell line. Some experiments were also conducted to dissect the underlying ionic and molecular mechanisms of OlyA/PlyB toxicity by modifying the ionic composition of the external medium and using pharmacological tools, respectively.

MATERIALS AND METHODS

Materials

The OlyA and PlyB proteins, purified from the oyster mushroom as previously described by Ota et al. (2013), were kindly provided by Peter Maček (University of Ljubljana, Slovenia). The mixture of OlyA/PlyB at a 9:1 molar ratio, which was based on the natural concentration ratio of these two proteins in mushroom, was dissolved in distilled water and stored in aliquots at -18°C. Verapamil, benzamil, sodium isethionate, lanthanum chloride, ethylene glycol tetraacetic acid, ionomycin, Orange plasma membrane stain, Fura-2 AM and Fluo-4 AM were purchased from Sigma-Aldrich Co. (St. Louis, Missouri, USA). Thapsigargin (TG) was purchased from Molecular Probes (Eugene, Oregon, USA). N-methyl-D-glucamine hydrochloride was purchased from Chemical Point (Deisenhofen, Germany). Sucrose was obtained from Merck (Darmstadt, Germany). The cell culture media and reagents were purchased from Sigma-Aldrich and Gibco®, Life Technologies (Breda, The Netherlands) unless otherwise specified.

Cultured NG108-15 cells

The mouse neuroblastoma×rat glioma NG108-15 cell line was purchased from the American Type Culture Collection (ATCC; LGC Standards GmbH, Wesel, Germany). The neuroblastoma cells were maintained in Dulbecco's modified Eagle medium (DMEM) supplemented with 5% fetal calf serum (FBS), 2% HAT (hypoxanthine 100 μM, aminopterin 0.4 μM, and thymidine 16 μM), Glutamax™-I 2 mM, glycine 3 μM, penicillin 100 IU/mL and streptomycin 100 μg/mL at 37°C in a humidified atmosphere with 5% (v/v) CO_2 as previously described (Rouzaire-Dubois and Dubois, 1990). To induce the differentiation of NG108-15 cells, they were first exposed to 2% dimethyl sulfoxide (DMSO) in the culture medium for 72 h. The DMSO-containing medium was then replaced with culture medium containing 1% FBS and 0.5 mM dibutyryl-cyclic adenosine monophosphate to achieve differentiation in 1-3 days. At the end of the differentiation period, the cells were washed twice with Dulbecco's phosphate-buffered saline (DPBS), pH 7.4, and treated as required in DPBS supplemented with $CaCl_2$, $MgCl_2$, glucose and pyruvate (sDPBS).

Confocal laser scanning microscopy

An inverted Leica multispectral laser scanning confocal microscope (Leica Microsystems, Heidelberg, Germany) was used for the neuronal morphology evaluation and calcium activity measurements in individual NG108-15 cells. The cells were trypsinized and plated into Lab-Tek™ 8-well borosilicate coverglasses (Thermo Scientific, Waltham, MA USA) at a density of 3 x 10^4 cells/well and differentiated as described above. For the morphology assessment, the NG108-15 cells were stained with the Orange plasma membrane stain (final concentration, 5 µg/ml) for 15 min at room temperature in the dark. Subsequently, the cells were gently rinsed three times with DPBS and treated with the OlyA/PlyB complex in sDPBS. The excitation of the Orange plasma membrane stain was achieved with the use of an excitation laser at 543 nm. An oil immersion objective lens (Leica, Planapo 40×N.A.=1.25) was used to obtain NG108-15 cell optical sections. The fluorescence emission was directed to the photomultiplier tube through a dichroic prism (488/543/633) and a 101.77-µm pinhole to create a confocal image. A series of optical sections were collected using a scanning format of 1024×1024 pixels. Each confocal section was obtained by 2-times integration of a single frame scan. A series of 1-µm optical sections was collected through the entire neuron before (time 0) and at 5, 10, 15, 30 and 60 min after the addition of OlyA/PlyB. The effects of OlyA/PlyB were quantified using the three-dimensional projected area as an index of cell volume as previously described (Meunier *et al.*, 2000). Leica digital image software was used for morphometric analysis.

$[Ca^{2+}]_i$ measurements

$[Ca^{2+}]_i$ was measured in individual cells and cell populations using an inverted Leica multispectral laser scanning confocal microscope and Mithras LB 940 multimode microplate reader (Berthold Technologies, Bad Wildbad, Germany), respectively. Differentiated NG108-15 cells grown on borosilicate coverglasses at the bottom of polystyrene chambers (Lab-Tek™ 8-well) were loaded with Fluo-4 AM (final concentration = 4 µM) in the dark at room temperature for 30 min. The fluorescence imaging was performed after three washes with sDPBS. To obtain the fluorescence signal of almost an entire cell, a large pinhole diameter (10 Airy disc) and an oil immersion objective lens (Leica, Planapo 40×, N.A.=1.25) were used. The photomultiplier gain was kept constant during the experiments.

A multimode microplate reader was used to measure the time-dependent effects of OlyA/PlyB on $[Ca^{2+}]_i$ in NG108-15 cell populations and to examine the mechanisms underlying the OlyA/PlyB-induced $[Ca^{2+}]_i$ changes. Differentiated NG108-15 cells were trypsinized, and the cell number was determined using a hemocytometer. The cells were resuspended in sDPBS at a density of 4 x 10^6/mL and loaded with 2.5 µM Fura-2/acetoxy-methyl ester (Fura-2 AM) dissolved in DMSO for 30 min at room temperature (22 ± 2°C). Subsequently, the Fura-2 AM was washed out, and the

cells were resuspended in sDPBS at a density of $2x10^6$/mL. The cells were then seeded into black 96-well plates at a density of ~$4x10^5$ cells/well. For the first 40 seconds (time resolution 0.5 sec), the baseline fluorescence was determined by calculating the ratio of the fluorescence emission intensity obtained at 510 nm with excitation at 340 nm and at 380 nm (ratio F_{340}/F_{380}). Subsequently, OlyA/PlyB was injected automatically, and the emission fluorescence intensity was measured for an additional 300 sec (time resolution 0.5 sec). All measurements were performed at 30°C within 2-3 hours after Fura-2 AM loading. The mean background fluorescence (baseline) was subtracted from the signal fluorescence. The changes in the F_{340}/F_{380} ratio were used as the index of variation in $[Ca^{2+}]_i$ (Grynkiewicz *et al.*, 1985).

Data analysis

The statistical analyses of the data were performed using Student's t-test (two-tailed) with Sigma Plot statistical software ver. 11. The values are expressed as the means ± S.E.M. The differences were considered significant at $p \leq 0.05$.

RESULTS

OlyA/PlyB induces NG108-15 cellular swelling

Confocal microscopic imaging of live, differentiated NG108-15 cells was used to evaluate the effect of OlyA/PlyB on the cell morphology. Utilizing the Orange plasma membrane stain, confocal microscopy revealed that 70 nM/7.8 nM OlyA/PlyB induced noticeable cellular swelling and the formation of spherical membrane protrusions, i.e. blebs. Membrane bleb formation was first noticed after 15 min of exposure to 70 nM/7.8 nM OlyA/PlyB, and by 30 to 60 min after the exposure, the size and number of blebs were increased (Fig. 1). The quantitative assessment of the OlyA/PlyB-induced effect on the cellular swelling is shown in Fig. 2. OlyA/PlyB induced a significant time- and concentration-dependent increase in the three-dimensional projected area of the NG108-15 cells, indicative of cellular swelling (Fig. 2). The significant increase in the three-dimensional projected area with respect to the controls was detected as early as 5 and 15 min after exposure to 70 nM/7.8 nM and 42 nM/4.7 nM OlyA/PlyB, respectively. The swelling was most evident after 60-min exposure to the higher concentration (70 nM/7.8 nM of OlyA/PlyB), as demonstrated by a 44% ± 3.1 increase in the projected area compared to the control ($n = 39$; $p < 0.01$). The lowest tested concentration of OlyA/PlyB (7 nM/0.78 nM) did not affect the NG108-15 cell morphology (Fig. 2) and did not induce membrane bleb formation (data not shown). A small, time-dependent increase in the projected areas of the NG108-15 cells was also observed under the control conditions (Fig. 2). Overall, the morphological results provide evidence supporting the OlyA/PlyB-

induced swelling of NG108-15 cells associated with plasma membrane bleb formation.

Next, we examined the possible mechanisms underlying the morphological responses induced by OlyA/PlyB in the NG108-15 cells. As shown in Fig. 3, equimolar substitution of extracellular NaCl with sucrose or Na-isethionate completely prevented the OlyA/PlyB-induced swelling of the NG108-15 cells. We also investigated whether the altered cell morphology was associated with a change in $[Ca^{2+}]_i$. The results show that a Ca^{2+}-depleted PBS or the presence of 10 μM benzamil, a potent $3Na^+/Ca^{2+}$ exchange (NCX) blocker, significantly reduced but did not completely prevent the OlyA/PlyB-induced effect on cell projected area (Fig. 3).

Effect of OlyA/PlyB on intracellular Ca^{2+} activity $[Ca^{2+}]_i$ in the NG108-15 cells under various experimental conditions

To determine whether the cellular swelling was indirectly associated with an influx of external Ca^{2+}, $[Ca^{2+}]_i$ measurements on individual NG108-15 cells and on cell populations were performed using the intracellular calcium indicators Fluo-4 AM and Fura-2 AM, respectively. As shown in Fig. 4, 1400 nM/156 nM OlyA/PlyB triggered a time-dependent increase in $[Ca^{2+}]_i$ in individual NG108-15 cells followed by a rapid decrease of the fluorescence (Fig. 4C), which was suggestive of cell lysis. A lower concentration of OlyA/PlyB (700 nM/78 nM) was therefore used in subsequent experiments monitoring $[Ca^{2+}]_i$ in the NG108-15 cell populations.

Fluorometric measurements of the NG108-15 cell populations then revealed that OlyA/PlyB, at concentrations ranging from 70 nM/7.8 nM to 350/39 nM OlyA/PlyB, had no significant effect on the $[Ca^{2+}]_i$, while 700 nM/78 nM OlyA/PlyB significantly increased the $[Ca^{2+}]_i$ ($p < 0.05$) (Fig. 5B). The OlyA/PlyB-induced increase in $[Ca^{2+}]_i$ was dependent on the presence of extracellular Ca^{2+} because this increase was eliminated in the Ca^{2+}-depleted medium (Fig. 5A).

Representative recordings of the OlyA/PlyB-induced time-dependent changes in the F_{340}/F_{380} ratio under different experimental conditions in populations of differentiated NG108-15 cells and the maximal changes in the F_{340}/F_{380} ratio at the 5-min time point are shown in Fig. 6 and 7, respectively. The NG108-15 cells responded to a depolarization induced by 70 mM KCl with a transient rise in $[Ca^{2+}]_i$ followed by sustained $[Ca^{2+}]_i$ elevation. The depolarization-induced rise in $[Ca^{2+}]_i$ was further enhanced by the addition of OlyA/PlyB (700 nM/78 nM) (Fig. 6A). In addition to the effects of the KCl-induced depolarization, which may be due to the inactivation of voltage-dependent calcium channels, the involvement of voltage-gated L-type Ca^{2+} channels in the OlyA/PlyB-induced $[Ca^{2+}]_i$ increase was examined using the L-type Ca^{2+} channel blocker, verapamil. As shown in Fig. 6B, 1 μM verapamil did not abolish the OlyA/PlyB-induced increase in $[Ca^{2+}]_i$. Although the response appeared to decrease, the effect was not significantly different from the $[Ca^{2+}]_i$ increase induced by 700 nM/78 nM OlyA/PlyB ($p > 0.05$) (Fig. 7). Similarly, the

presence of lanthanum chloride (0.5 mM), which selectively inhibits Ca^{2+} influx by blocking the voltage-sensitive Ca^{2+} channels in the neuroblastoma cell line at low concentrations (Kasai and Neher, 1992), did not significantly prevent the increase in $[Ca^{2+}]_i$ induced by 700 nM/78 nM OlyA/PlyB (Fig. 6C and Fig. 7; $p > 0.05$).

To evaluate the role of intracellular Ca^{2+} stores in the OlyA/PlyB-induced increase in $[Ca^{2+}]_i$, we used thapsigargin, a specific inhibitor of endoplasmic Ca^{2+}-adenosine 5′-triphosphatase (Ca^{2+}-ATPase) that results in the depletion of intracellular Ca^{2+} stores (Kostyuk and Verkhratsky, 1994). As shown in Fig. 6D, thapsigargin partially inhibited the OlyA/PlyB-induced increase in $[Ca^{2+}]_i$. However, the decrease was not statistically significant ($p > 0.05$) (Fig. 7). Equimolar replacement of the extracellular Na^+ and Cl^- by *N*-methyl-D-glucamine efficiently prevented the increase in $[Ca^{2+}]_i$ induced by 700 nM/78 nM OlyA/PlyB (Fig. 6E and Fig. 7). Benzamil (10 μM), an inhibitor of NCX, also significantly reduced the response to 700 nM/78 nM OlyA/PlyB as indicated by the significant ($p < 0.05$) reduction of the maximal F_{340}/F_{380} ratio (Fig. 6F and Fig. 7).

The maximal F_{340}/F_{380} fluorescence response triggered by 700 nM/78 nM OlyA/PlyB was approximately 50% lower than the response induced by 5 μM ionomycin, a Ca^{2+} ionophore (Fig. 7).

DISCUSSION

Confocal microscopy was used to directly examine the morphological responses induced by OlyA/PlyB in differentiated NG108-15 cells. The results showed that OlyA/PlyB increased the three-dimensional projected area of the neuroblastoma NG108-15 cells and that the cellular swelling was partially dependent on the presence of extracellular Ca^{2+}. The cellular projected area change was accompanied by the formation of prominent plasma membrane blebs. Plasma membrane injury and formation of protrusions often reflect cell injury leading to necrotic cell death (Babiychuk *et al.*, 2011). The sustained influx of extracellular Ca^{2+} through an injured plasma membrane causes plasma membrane blebbing. A very recent publication showed that OlyA/PlyB forms non-selective ion pores in the plasma membranes of neuroblastoma N18 and CHO cells (Schlumberger *et al.*, 2014), which allowed influx of extracellular Ca^{2+} and consequent bleb formation. This phenomenon has also been shown to occur in response to several other proteins, including the bacterial pore-forming toxins streptolysin O (Keyel *et al.*, 2011) and parasporin-2 (Kitada *et al.*, 2009). However, the concentrations of OlyA/PlyB (42 nM/4.7 nM - 70 nM/7.8 nM) that induced intracellular edema and plasma membrane blebbing of NG108-15 cells did not significantly increase the $[Ca^{2+}]_i$. Therefore, a mechanism other than an increase in $[Ca^{2+}]_i$ may be responsible for the plasma membrane bleb formation that was observed in NG108-15 cells exposed to nanomolar concentrations of OlyA/PlyB. On one hand, the development of blebs in the presence

of OlyA/PlyB may be related to other membrane permeability changes since, in inner hair cells, blebbing has been associated with raised intracellular Na^+ concentration (Shi *et al.*, 2005). On the other hand, the vesiculation phenomenon is mainly linked to OlyA, which is *per se* non-lytic and is responsible for the initial membrane binding of the OlyA/PlyB complex (Ota *et al.*, 2013; Skocaj *et al.*, 2014). Similar to streptolysin (Keyel *et al.*, 2011), OlyA can induce vesiculation in living cells and in artificial lipid vesicles, suggesting that vesicle formation is a result of a direct physical effect of these proteins on the plasma membrane. Non-excitable MDCK cells treated with low concentrations of fluorescently tagged OlyA revealed unchanged cell morphology after up to 3 days of incubation with a 1 µM concentration of the protein (Skocaj *et al.*, 2014). The fact that these vesicles were clearly stained with fluorescently tagged OlyA suggests that they sequester this protein and help in its clearance, which could explain the difference in the concentrations of OlyA/PlyB that are needed to increase the $[Ca^{2+}]_i$ compared to those that are required to induce swelling and bleb formation.

The OlyA/PlyB-induced swelling of NG108-15 cells was significantly reduced when Ca^{2+} was withdrawn from the external solution. In addition, the presence of the potent NCX selective exchange blocker, benzamil, had moderate protective effects against the cellular swelling. These results strongly suggest that an entry of Ca^{2+} through NCX may be involved in the OlyA/PlyB-induced swelling of NG108-15 cells. Surprisingly, equimolar replacement of NaCl by sucrose or the organic sodium salt Na-isethionate completely prevented the OlyA/PlyB-induced swelling of NG108-15 cells, which is in contrast to what was previously reported for N18 cells (Schlumberger *et al.*, 2014). In fact, there are some discrepancies between the OlyA/PlyB-induced increase in the three-dimensional projected area of NG108-15 cells (present study) and the OlyA/PlyB-formed pores in N18 cells (Schlumberger *et al.*, 2014). In particular, the effective concentrations are quite different since OlyA/PlyB concentrations of between 0.042 µM/0.0047 µM and 0.07 µM/0.0078 µM were enough to produce swelling of NG108-15 cells whereas slightly higher concentrations (i.e. 0.054 µM/0.006 µM) showed inefficacy to form pores in N18 cells, despite the fact that OlyA and PlyB were mixed at a 90%/10% ratio in both cases. It is worth noting that, when applied to N18 cells at 0.054 µM/0.006 µM, OlyA/PlyB did not form membrane pores, i.e. no detectable increase occurred in the current recorded at a holding potential of -50 mV (Benoit E., personal communication). Although sensibility differences to OlyA/PlyB effects between the two types of cells may explain such discrepancies, it is unlikely that the swelling of NG108-15 cells was consequent to perturbation of the osmotic equilibrium between intra- and extracellular media as a result of pore formation. Hence, our data show that a cellular swelling was observed in the presence of 0.07 µM/0.0078 µM OlyA/PlyB while no increased $[Ca^{2+}]_i$ was detected in these cells in the presence of between 0.07 µM/0.0078 µM and 0.35 µM/0.039 µM OlyA/PlyB, despite the fact that

Ca^{2+} was reported to flow through the OlyA/PlyB-formed pores in N18 cells (Schlumberger *et al.*, 2014). In addition, NG108-15 cell swelling did not occurred when NaCl was substituted by Na-isethionate, which would suggest that isethionate ions (ionic radius of 0.301 nm; Smith *et al.*, 1999) do not flow through OlyA/PlyB-formed pores. However, bigger anions, such as gluconate (ionic radius of 0.376 nm; Smith *et al.*, 1999), were reported to flow through the OlyA/PlyB-formed pores in N18 cells (Schlumberger *et al.*, 2014). The hydrodynamic radius of OlyA/PlyB pores formed in N18 cells (2.7 µM/0.3 µM) and bovine red blood cells (0.45 µM/0.05 µM) were estimated to be 2.45 nm and 3.78 nm, respectively. Consistent with this, OlyA/PlyB formed non-selective ion pores in the plasma membranes of N18 cells, *i.e.* allowing no preferential selectivity for cations over anions. In contrast, polyethylene-glycol 8000 (hydrodynamic radius of 3.78 nm) provided almost complete osmotic protection against erythrocyte haemolysis (Schlumberger *et al.*, 2014). Although it is unlikely that the OlyA/PlyB-induced swelling of NG108-15 cells was consequent to pore formation, one cannot exclude the possibility that, in these cells, the hydrodynamic radius of OlyA/PlyB-formed pores is smaller and their ion selectivity different when compared to N18 cells. To definitively conclude, further experiments would be needed to determine the selectivity and to estimate the hydrodynamic radius of OlyA/PlyB-formed pores in NG108-15 cells. In particular, it would be interesting to check whether the pore hydrodynamic radius is smaller than the ionic radii of isethionate and sucrose (i.e. 0.301 and 0.44 nm, respectively).

In contrast to the cellular swelling, the increased $[Ca^{2+}]_i$ that occurred in NG108-15 cells, in the presence of 0.7 µM/0.078 µM OlyA/PlyB, is likely to involve the formation of OlyA/PlyB pores in these cells. Hence, Ca^{2+} entry is known to activate Ca^{2+}-induced Ca^{2+} release (CICR) in neurons *via* ryanodine receptors located in the endoplasmic reticulum membrane (Verkhratsky and Shmigol, 1996). To examine whether Ca^{2+} release from internal stores also contributed to the OlyA/PlyB-induced $[Ca^{2+}]_i$ increase, thapsigargin was used. This inhibitor discharges the intracellular Ca^{2+} stores by specific inhibition of the endoplasmic reticulum Ca^{2+}-ATPase (Thastrup *et al.*, 1990). In NG108-15 cells, the OlyA/PlyB-induced increase in the $[Ca^{2+}]_i$ was unaffected by pretreatment with thapsigargin, indicating that the $[Ca^{2+}]_i$ increase was primarily due to the influx of extracellular Ca^{2+}. On the basis that the OlyA/PlyB complex forms non-selective ion channels in the membranes of the neuroblastoma N18 cells (Schlumberger *et al.*, 2014), plasma membrane depolarization may induce Ca^{2+} entry through the voltage-dependent L- and N-type Ca^{2+} channels. However, the OlyA/PlyB-induced increase in the $[Ca^{2+}]_i$ in the differentiated NG180-15 cells was not significantly inhibited by either verapamil, an L-type channel blocker, or low concentration of $LaCl_3$, which blocks the calcium channels in neuroblastoma cells, suggesting that the OlyA/PlyB-mediated Ca^{2+} influx occurs through other Ca^{2+} entry pathways. Additionally, depolarization with 70 mM KCl did not significantly modify either the time course or the amplitude of the increase in

the $[Ca^{2+}]_i$ induced by OlyA/PlyB. During a potassium-induced plasma membrane depolarization, almost all L-type channels should be inactivated; therefore, it appears unlikely that OlyA/PlyB-induced Ca^{2+} entry occurred through voltage-dependent Ca^{2+} channels. Another possible mediator for the OlyA/PlyB-triggered increase in $[Ca^{2+}]_i$ may be the $3Na^+/Ca^{2+}$ exchange NCX (Blaustein and Lederer, 1999). To test this possibility, experiments were performed with a specific NCX blocker, benzamil. These experiments confirmed that benzamil, as well as iso-osmolar substitution of external Na^+ with the plasma membrane-impermeant cation *N*-methyl-D-glucamine, significantly reduced Ca^{2+} entry into the neuroblastoma NG108-15 cells, suggesting an important role for NCX in the OlyA/PlyB-induced increase in $[Ca^{2+}]_i$. Under these conditions, Na^+ influx through OlyA/PlyB non-selective ion pores will activate NCX to operate in the opposite direction, thus contributing to the increase in the $[Ca^{2+}]_i$ triggered by OlyA/PlyB. Finally, it is likely that Ca^{2+} influx occurred also through the pores formed by OlyA/PlyB in the plasma membrane of neuroblastoma cells (see Schlumberger *et al.*, 2014).

To our knowledge, this work is the first demonstration of the OlyA/PlyB-induced swelling and plasma membrane blebbing of neuroblastoma NG108-15 cells. Formation of cellular edema requires the presence of Na^+ and/or Cl^- in the extracellular space and may be related to an influx of Na^+ and/or a shift in Cl^-, which induce a marked influx of water that is ultimately responsible for cellular swelling. In addition, OlyA/PlyB also induced Ca^{2+} influx into the NG108-15 cells. A switch in the NCX mode to mediate Ca^{2+} influx, associated with the *de novo* formation of non-selective ion pores by OlyA/PlyB in plasma membranes of mammalian cells, appears to play an important role in this effect. In conclusion, our data demonstrate that the OlyA/PlyB complex affected the neuroblastoma NG108-15 cell morphology and Ca^{2+} homeostasis and describe the possible mechanisms underlying this toxic action. The described morphological effects and the underlying cellular mechanisms responsible for these observations are important steps towards understanding the toxic cardiorespiratory effects of the OlyA/PlyB protein complex *in vivo*.

Acknowledgements

The authors would like to thank Professor Peter Maček for critical reading of the manuscript, American Journal Experts (AJE) for English language editing and Katarina Babnik for her excellent technical assistance. This study was financially supported by the Slovenian Research Agency program P4-0053.

REFERENCES

Al-Deen, I. H., Twaij, H. A., Al-Badr, A. A., and Istarabadi, T. A. (1987). Toxicologic and histopathologic studies of *Pleurotus ostreatus* mushroom in mice. *J Ethnopharmacol* **21**, 297-305.

Babiychuk, E. B., Monastyrskaya, K., Potez, S., and Draeger, A. (2011). Blebbing confers resistance against cell lysis. *Cell Death Differ* **18**, 80-9.

Berne, S., Krizaj, I., Pohleven, F., Turk, T., Macek, P., and Sepcic, K. (2002). *Pleurotus* and *Agrocybe* hemolysins, new proteins hypothetically involved in fungal fruiting. *Biochim Biophys Acta* **1570**, 153-9.

Berne, S., Sepcic, K., Anderluh, G., Turk, T., Macek, P., and Poklar Ulrih, N. (2005). Effect of pH on the pore forming activity and conformational stability of ostreolysin, a lipid raft-binding protein from the edible mushroom *Pleurotus ostreatus*. *Biochemistry* **44**, 11137-47.

Berne, S., Lah, L., and Sepcic, K. (2009). Aegerolysins: structure, function, and putative biological role. *Protein Sci* **18**, 694-706.

Blaustein, M. P., and Lederer, W. J. (1999). Sodium/calcium exchange: its physiological implications. *Physiol Rev* **79**, 763-854.

Gilbert, R. J., Mikelj, M., Dalla Serra, M., Froelich, C. J., and Anderluh, G. (2013). Effects of MACPF/CDC proteins on lipid membranes. *Cell Mol Life Sci* **70**, 2083-98.

Grynkiewicz, G., Poenie, M., and Tsien, R. Y. (1985). A new generation of Ca^{2+} indicators with greatly improved fluorescence properties. *J Biol Chem* **260**, 3440-50.

Hirst, R. A., Kadioglu, A., O'Callaghan, C., and Andrew, P. W. (2004). The role of pneumolysin in pneumococcal pneumonia and meningitis. *Clin Exp Immunol* **138**, 195-201.

Juntes, P., Rebolj, K., Sepcic, K., Macek, P., Zuzek, M. C., Cestnik, V., and Frangez, R. (2009). Ostreolysin induces sustained contraction of porcine coronary arteries and endothelial dysfunction in middle- and large-sized vessels. *Toxicon* **54**, 784-92.

Kasai, H., and Neher, E. (1992). Dihydropyridine-sensitive and omega-conotoxin-sensitive calcium channels in a mammalian neuroblastoma-glioma cell line. *J Physiol* **448**, 161-88.

Keyel, P. A., Loultcheva, L., Roth, R., Salter, R. D., Watkins, S. C., Yokoyama, W. M., and Heuser, J. E. (2011). Streptolysin O clearance through sequestration into blebs that bud passively from the plasma membrane. *J Cell Sci* **124**, 2414-23.

Kitada, S., Abe, Y., Maeda, T., and Shimada, H. (2009). Parasporin-2 requires GPI-anchored

proteins for the efficient cytocidal action to human hepatoma cells. *Toxicology* **264**, 80-8.

Kostyuk, P., and Verkhratsky, A. (1994). Calcium stores in neurons and glia. *Neuroscience* **63**, 381-404.

Meunier, F. A., Frangez, R., Benoit, E., Ouanounou, G., Rouzaire-Dubois, B., Suput, D., and Molgo, J. (2000). Ca^{2+} and Na^{+} contribute to the swelling of differentiated neuroblastoma cells induced by equinatoxin-II. *Toxicon* **38**, 1547-60.

Orihuela, C. J., Gao, G., Francis, K. P., Yu, J., and Tuomanen, E. I. (2004). Tissue-specific contributions of pneumococcal virulence factors to pathogenesis. *J Infect Dis* **190**, 1661-9. Nagahama, M., and Sakurai, J. (1991). Distribution of labeled *Clostridium perfringens* epsilon toxin in mice. *Toxicon* **29**, 211-7.

Ota, K., Leonardi, A., Mikelj, M., Skocaj, M., Wohlschlager, T., Kunzler, M., Aebi, M., Narat, M., Krizaj, I., Anderluh, G., Sepcic, K., and Macek, P. (2013). Membrane cholesterol and sphingomyelin, and ostreolysin A are obligatory for pore-formation by a MACPF/CDC-like pore-forming protein, pleurotolysin B. *Biochimie* **95**, 1855-64.

Ota, K., Butala, M., Viero, G., Dalla Serra, M., Sepcic, K., and Macek, P. (2014). Fungal MACPF-like proteins and aegerolysins: bi-component pore-forming proteins? *Subcell Biochem* **80**, 271-91.

Rebolj, K., Ulrih, N. P., Macek, P., and Sepcic, K. (2006). Steroid structural requirements for interaction of ostreolysin, a lipid-raft binding cytolysin, with lipid monolayers and bilayers. *Biochim Biophys Acta* **1758**, 1662-70.

Rebolj, K., Batista, U., Sepcic, K., Cestnik, V., Macek, P., and Frangez, R. (2007). Ostreolysin affects rat aorta ring tension and endothelial cell viability in vitro. *Toxicon* **49**, 1211-3.

Rebolj, K., Bakrac, B., Garvas, M., Ota, K., Sentjurc, M., Potrich, C., Coraiola, M., Tomazzolli, R., Dalla Serra, M., Macek, P., and Sepcic, K. (2010). EPR and FTIR studies reveal the importance of highly ordered sterol-enriched membrane domains for ostreolysin activity. *Biochim Biophys Acta* **1798**, 891-902.

Rouzaire-Dubois, B., and Dubois, J. M. (1990). Tamoxifen blocks both proliferation and voltage-dependent K^{+} channels of neuroblastoma cells. *Cell Signal* **2**, 387-93.

Schlumberger, S., Kristan, K. C., Ota, K., Frangez, R., Molgomicron, J., Sepcic, K., Benoit, E., and Macek, P. (2014). Permeability characteristics of cell-membrane pores induced by ostreolysin A/pleurotolysin B, binary pore-forming proteins from the oyster mushroom. *FEBS Lett* **588**, 35-40.

Sepcic, K., Berne, S., Potrich, C., Turk, T., Macek, P., and Menestrina, G. (2003). Interaction of ostreolysin, a cytolytic protein from the edible mushroom *Pleurotus ostreatus*, with lipid membranes and modulation by lysophospholipids. *Eur J Biochem* **270,** 1199-210.

Sepcic, K., Berne, S., Rebolj, K., Batista, U., Plemenitas, A., Sentjurc, M., and Macek, P. (2004). Ostreolysin, a pore-forming protein from the oyster mushroom, interacts specifically with membrane cholesterol-rich lipid domains. *FEBS Lett* **575**, 81-5.

Shi, X., Gillespie, P.G., and Nuttall, A.L. (2005). Na^+ influx triggers bleb formation on inner hair cells. *Am J Physiol Cell Physiol* **288,** C1332-C1341.

Skocaj, M., Resnik, N., Grundner, M., Ota, K., Rojko, N., Hodnik, V., Anderluh, G., Sobota, A., Macek, P., Veranic, P., and Sepcic, K. (2014). Tracking cholesterol/sphingomyelin-rich membrane domains with the ostreolysin A-mCherry protein. *PLoS One* **9**, e92783, doi: 10.1371/journal.pone.0092783.

Smith, S.S., Steinle, E.D., Meyerhoff, M.E., and Dawson, D.C. (1999). Cystic fibrosis transmembrane conductance regulator. Physical basis for lyotropic anion selectivity patterns. *J Gen Physiol* **114,** 799-818.

Soler-Jover, A., Blasi, J., Gomez de Aranda, I., Navarro, P., Gibert, M., Popoff, M. R., and Martin-Satue, M. (2004). Effect of epsilon toxin-GFP on MDCK cells and renal tubules in vivo. *J Histochem Cytochem* **52**, 931-42.

Thastrup, O., Cullen, P. J., Drobak, B. K., Hanley, M. R., and Dawson, A. P. (1990). Thapsigargin, a tumor promoter, discharges intracellular Ca^{2+} stores by specific inhibition of the endoplasmic reticulum Ca^{2+}-ATPase. *Proc Natl Acad Sci U S A* **87**, 2466-70.

Verkhratsky, A., and Shmigol, A. (1996). Calcium-induced calcium release in neurones. *Cell Calcium* **19**, 1-14.

Zuzek, M. C., Macek, P., Sepcic, K., Cestnik, V., and Frangez, R. (2006). Toxic and lethal effects of ostreolysin, a cytolytic protein from edible oyster mushroom (*Pleurotus ostreatus*), in rodents. *Toxicon* **48**, 264-71.

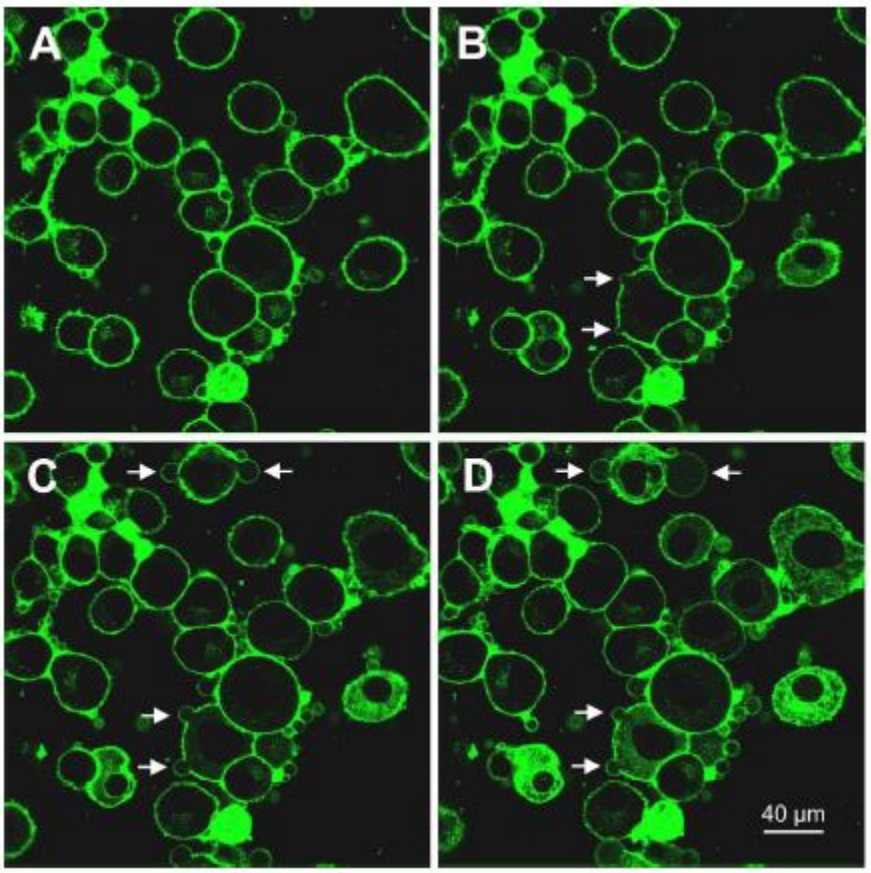

Figure 1. Effect of OlyA/PlyB on NG108-15 cell morphology. The same cluster of differentiated NG108-15 cells under control conditions (A) and at 15 min (B), 30 min (C) and 60 min (D) after the addition of OlyA/PlyB (70 nM/7.8 nM). Note the marked cellular swelling and the formation of plasma membrane blebs (arrows) induced by OlyA/PlyB. Scale bar, 40 µm.

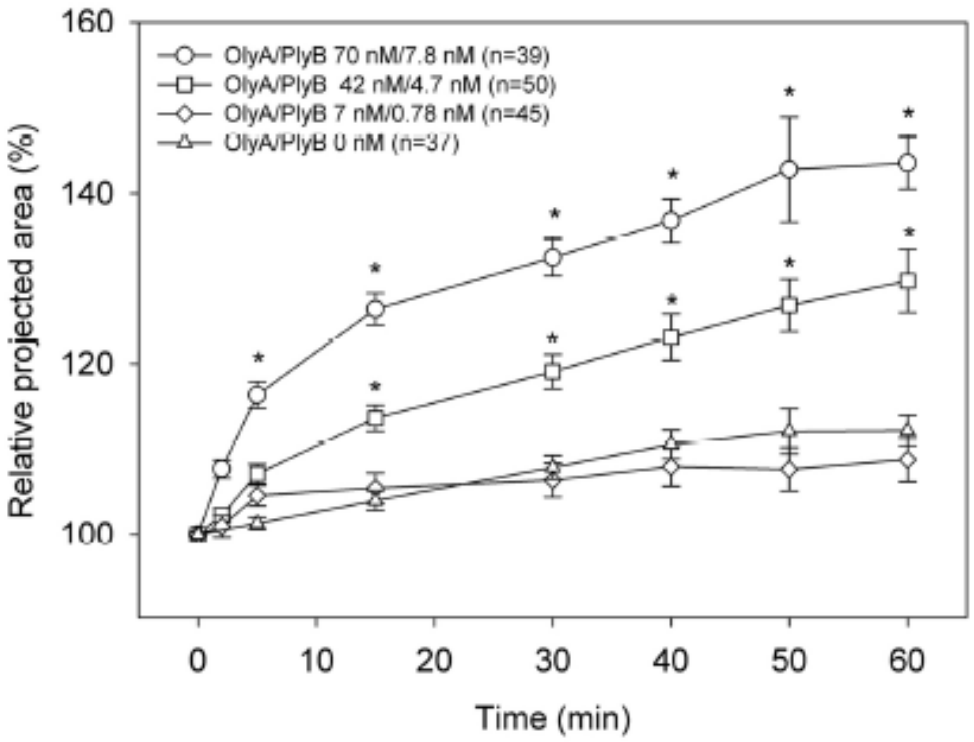

Figure 2. Time- and concentration–dependent effects of OlyA/PlyB on the three-dimensional projected area of NG108-15 cells. The data were normalized and expressed as the relative projected area with respect to the controls. Note the progressive and significant increase in the projected area of the NG108-15 cells induced by 42 nM/4.7 nM and 70 nM/7.8 nM OlyA/PlyB. The data are expressed as the means ± S.E.M.; n denotes the number of cells analyzed.* indicates $p < 0.05$ compared with the untreated NG108-15 cells.

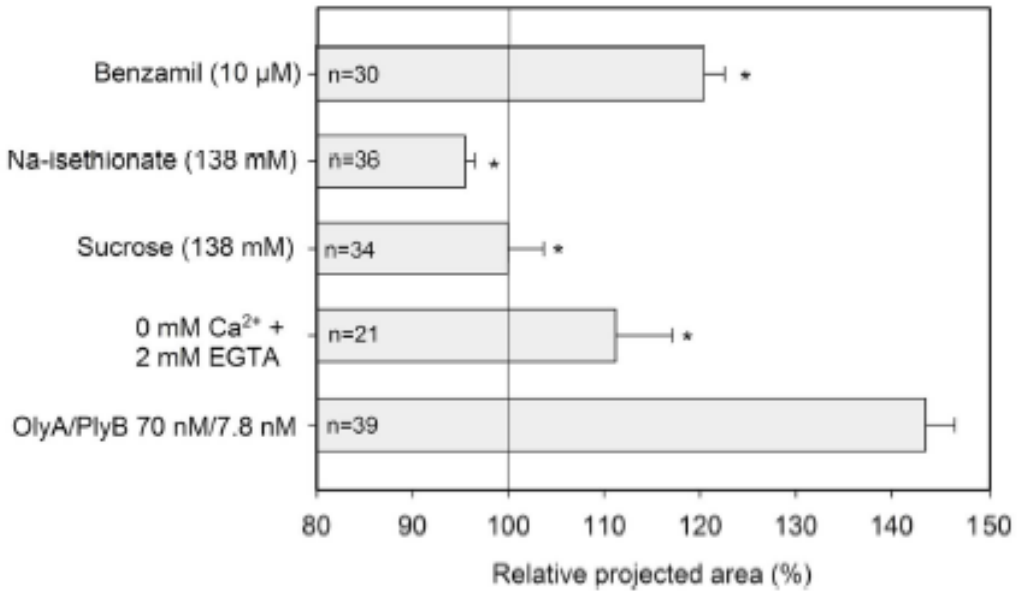

Figure 3. Effect of OlyA/PlyB on the three-dimensional projected area of the NG108-15 cells under various experimental conditions. The results shown are the changes in the relative projected area of NG108-15 cells exposed to OlyA/PlyB (60 min; 70 nM/7.8 nM) in the standard solution and the changes in the relative projected area of NG108-15 cells under the indicated conditions. Note that when NaCl was substituted with equimolar concentrations of either Na-isethionate or sucrose, no OlyA/PlyB-induced increase in the projected area of NG108-15 cells was detected, while the Ca^{2+}-depleted solution supplemented with EDTA or the solution containing the NCX blocker benzamil only partially prevented OlyA/PlyB-induced cellular swelling. Each column represents the means ± S.E.M.; n denotes the number of cells analyzed. * indicates $p < 0.05$ compared with the OlyA/PlyB-exposed NG108-15 cells.

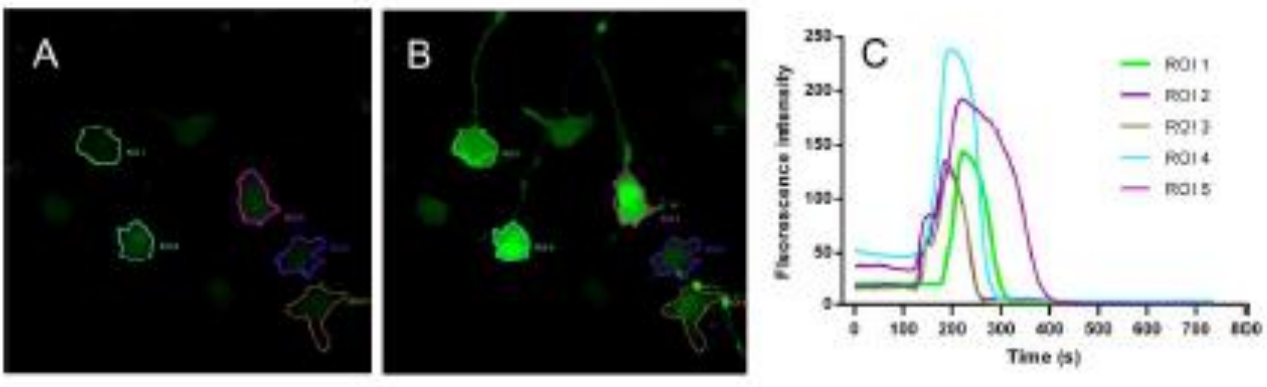

Figure 4. **OlyA/PlyB induces changes in intracellular Ca^{2+} activity $[Ca^{2+}]_i$ in individual NG108-15 cells.** Images of the Fluo-4 AM fluorescence (A) before (basal) and (B) during the action of 1400 nM/156 nM OlyA/PlyB. Note that after the addition of OlyA/PlyB, a strong increase in fluorescence was observed in the nuclear region and in the cytosol of the NG108-15 cells. (C) The time-course traces of the fluorescence intensity changes of selected NG108-15 cells corresponding to the regions of interest (ROIs) in panels A and B.

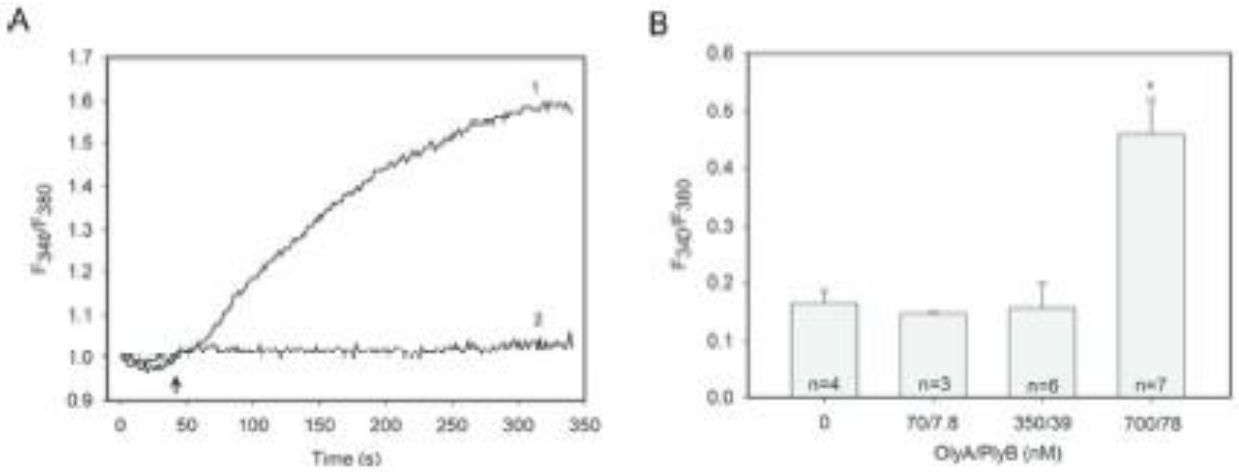

Figure 5. The effect of OlyA/PlyB on intracellular Ca^{2+} activity $[Ca^{2+}]_i$ in NG108-15 cells. (A) Time-dependent changes in the F_{340}/F_{380} ratio during the exposure of NG108-15 cells loaded with Fura-2 AM in standard solution with Ca^{2+} (trace 1) or with a nominally Ca^{2+}-free solution supplemented with 2 mM EGTA (trace 2) to 700 nM/78 nM OlyA/PlyB. Note in (1) the increase in the F_{340}/F_{380} ratio after the application of OlyA/PlyB (arrow) and the absence of a response (2) in the absence of external Ca^{2+}. The data shown are from a single representative experiment. (B) Maximal concentration-dependent OlyA/PlyB-induced increase in the F_{340}/F_{380} ratio, an index of the variation of $[Ca^{2+}]_i$, at the 5-min time point. Each column represents the means ± S.E.M. from three to seven independent experiments compared with untreated (control) NG108-15 cells (* indicates $p < 0.05$).

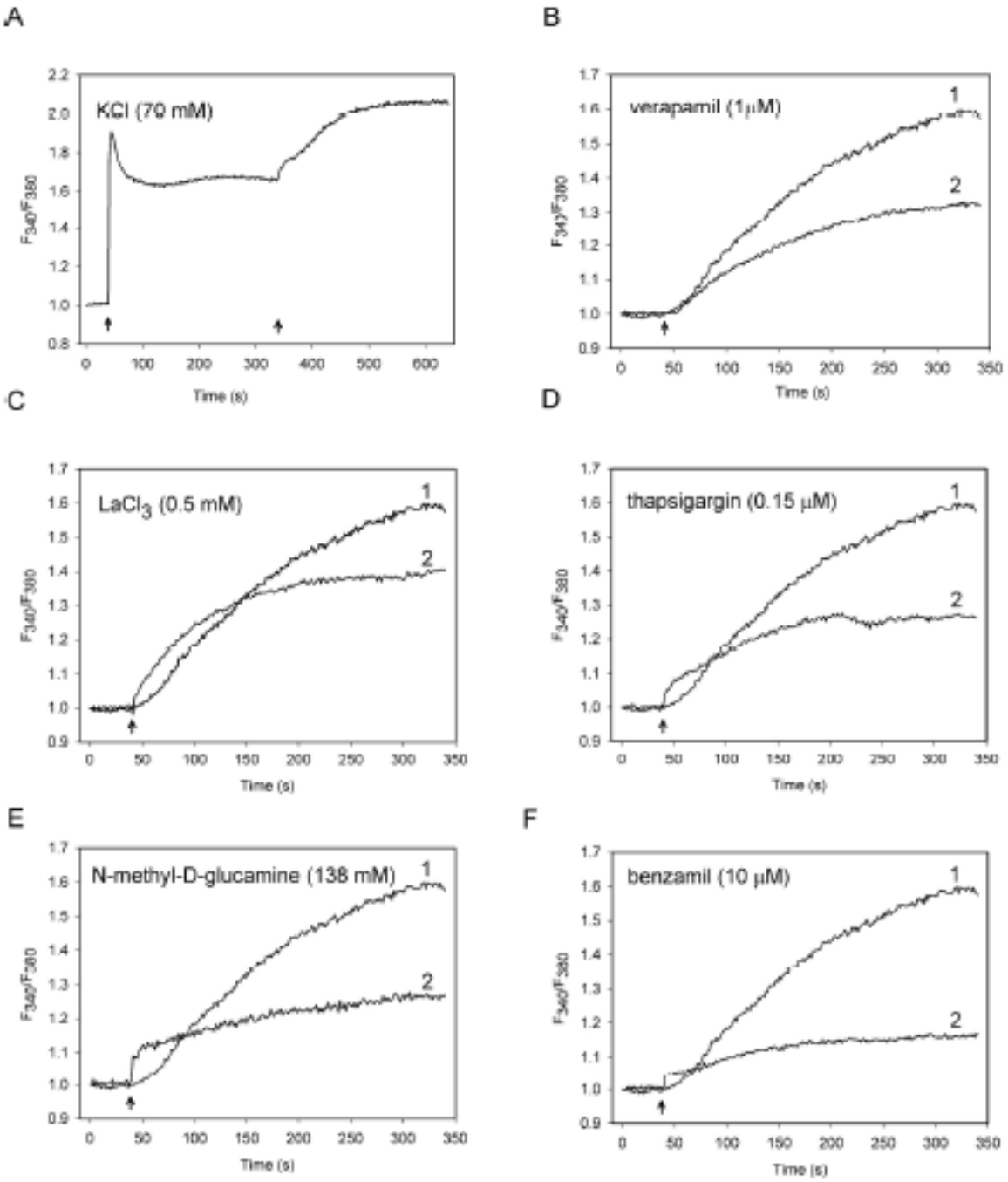

Figure 6. Representative recordings of the time-dependent changes in the F_{340}/F_{380} ratio induced by OlyA/PlyB in NG108-15 cells under various experimental conditions. The data show the time-dependent changes in the F_{340}/F_{380} ratio during the responses to 700 nM/78 nM OlyA/PlyB in NG108-15 cells loaded with Fura-2 AM in the standard solution with Ca^{2+} (trace 1 in panels B-F) and under the indicated conditions (trace 2 in panels B-F). Note the decreased response under all experimental conditions, in contrast to the KCl-induced potentiation of the effect. The time of OlyA/PlyB application is marked by an arrow.

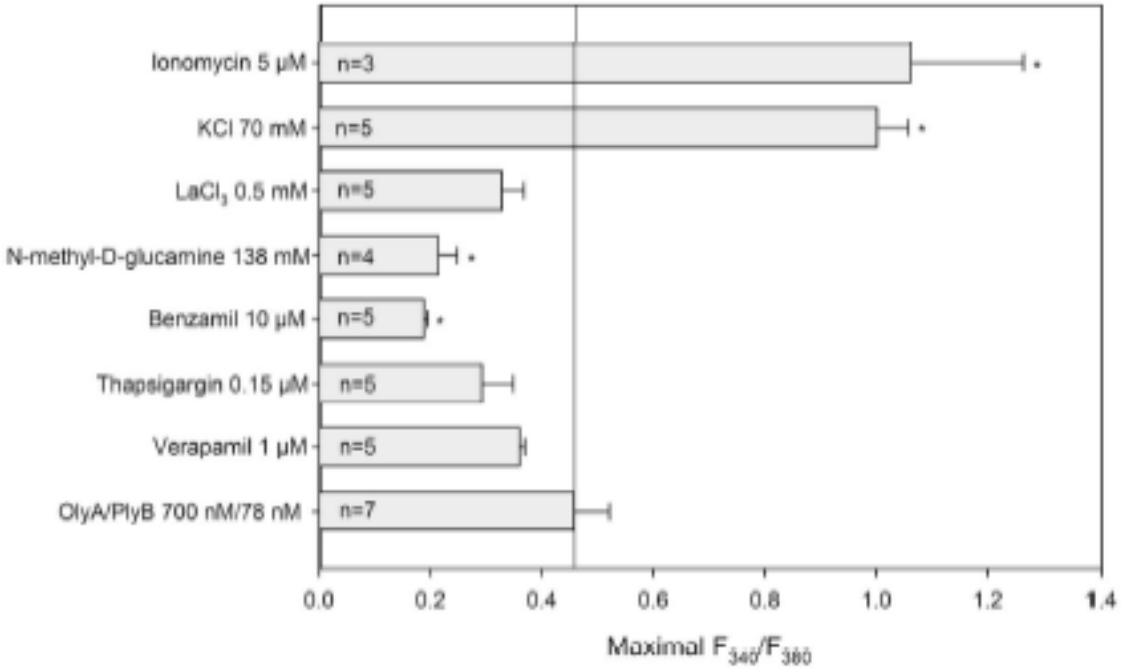

Figure 7. Maximal OlyA/PlyB-induced changes in the F_{340}/F_{380} fluorescence ratio under various experimental conditions in NG108-15 cells. The data shown are the responses of NG108-15 cells when exposed for 5 min to 5 µM ionomycin alone, 70 mM KCl and 700 nM/78 nM OlyA/PlyB or 700 nM/78 nM OlyA/PlyB following pretreatment for 30 min at room temperature with 0.5 mM $LaCl_3$, 10 µM benzamil, 0.15 µM thapsigargin or 1 µM verapamil in sDPBS. The concentrations of these agents were maintained during the 5-min exposure to 700 nM/78 nM OlyA/PlyB. The experiments were also performed using medium in which NaCl was substituted by N-methyl–D-glucamine (138 mM). Each column represents the means ± S.E.M. from three to seven independent experiments. * indicates $p < 0.05$ compared with the OlyA/PlyB-exposed NG108-15 cells.